Supporting Information for

Diel Redox Cycle of Manganese in the Surface Arctic Ocean

Y. Xiang*, P. J. Lam, J. M. Lee

Department of Ocean Sciences, University of California, Santa Cruz, CA 95064 USA

Contents of this file

Text S1
Figures S1 to S7
Tables S2 and S3

Additional Supporting Information (Files uploaded separately)

Captions for Tables S1 and S4
Tables S1 and S4 (uploaded separately)

Introduction

The supporting information for this paper consists of three main elements: a detailed description of the method used to find three Mn reference minerals, seven supplemental figures, four supplemental tables (two uploaded separately). Supplemental tables contain information about the light conditions, particulate Mn concentrations, Mn XANES reference and sample spectra, and Mn average oxidation states derived from the synchrotron analysis.

Text S1.

Overall, there are 18 Mn mineral references in our library (Table S3), including spectra of Mn minerals that we collected at Beamline 11-2 (e.g., pyroxmangite ($Mn^{II}SiO_3$), hureaulite ($Mn^{II}_5(PO_3OH)_2(PO_4)_2 \cdot 4H_2O$)), those shared by collaborators (e.g., δ-$Mn^{IV}O_2$, feitknechtite ($Mn^{III}OOH$), Mn(II)-citrate), and the most reduced surface sample, GT11010s at Station 26, which was smoothed using a smoothing parameter of 2 using SIXPACK. Linear combination fitting (LCF) of sample XANES spectra (Table S4) in the energy range of 6520-6600 eV was conducted using different combinations of Mn mineral references using the Least Sq. Fitting module in SIXPACK (Webb, 2005). The goodness of the LSF fit was evaluated by the magnitude of the R-factor (Newville, 2001). The particulate Mn (pMn) average oxidation state (AOS) was calculated as a weighted average of Mn(II), Mn(III), and Mn(IV) using the LCF fractions of three end-member Mn references chosen to represent each oxidation state. The Mn references used as end members for AOS calculations were GT11010s-Mn(II), feitknechtite ($Mn^{III}OOH$), and δ-$Mn^{IV}O_2$. We chose these three Mn reference minerals for the following two reasons. First, compared to the most reduced surface sample GT11010s, none of the other Mn(II) references in our library, including a number of Mn silicates and Mn-organic ligand complexes, showed the characteristic absorption peak at 6551 eV as seen in surface pMn samples in the Arctic Ocean (Figure S6 & Table S2). Secondly, to choose appropriate oxidized Mn mineral references for our surface Arctic dataset, we applied LCF to the XANES spectrum of a pMn sample from the dark halocline (GT10800s; 176 m at Station 14) thought to be dominated by oxidized pMn (c.f., Xiang & Lam, 2020), also analyzed at Beamline 11-2. The LCF of this sample with two endmembers, feitknechtite ($Mn^{III}OOH$) and δ-$Mn^{IV}O_2$, led to a low R factor (Newville, 2001) of 7.56×10^{-4} (Figure S4), suggesting that these two references are reasonable choices to represent Mn(III) and Mn(IV) in the Western Arctic Ocean. Indeed,

feitknechtite ($Mn^{III}OOH$), and δ-$Mn^{IV}O_2$ are commonly used as Mn(III/IV) reference compounds in

lab settings (Learman et al., 2011) and other ocean environments (Hermans et al., 2019; Lee et al.,

2021; Oldham et al., 2021). We also would like to note that the primary purpose of calculating

AOS is to define a metric to describe the variation in the speciation of pMn in the surface Arctic,

rather than to give an accurate and precise estimate of pMn AOS. Given the lack of sample

duplicates and beam time, the uncertainties in the values of pMn AOS calculated from the XANES

spectra could not be formally assessed during this study. However, major variations in spectral

features are clear and consistent with the trend of calculated pMn AOS (Figure 3).
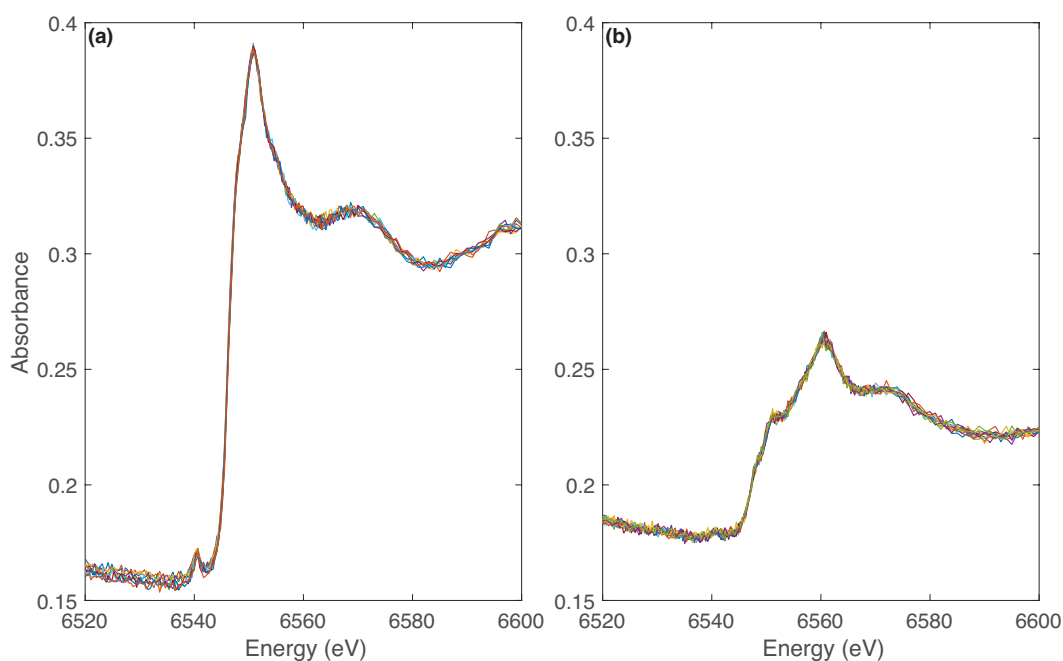

Figure S1. Raw Mn spectra of (a) one reduced pMn sample at Station 19 (9 scans over 1.5 hours) and (b) one oxidized sample at Station 48 (12 scans over 2 hours). No obvious energy shifts were observed in either sample over the course of the analyses, indicating no clear X-ray beam-induced photoreduction.
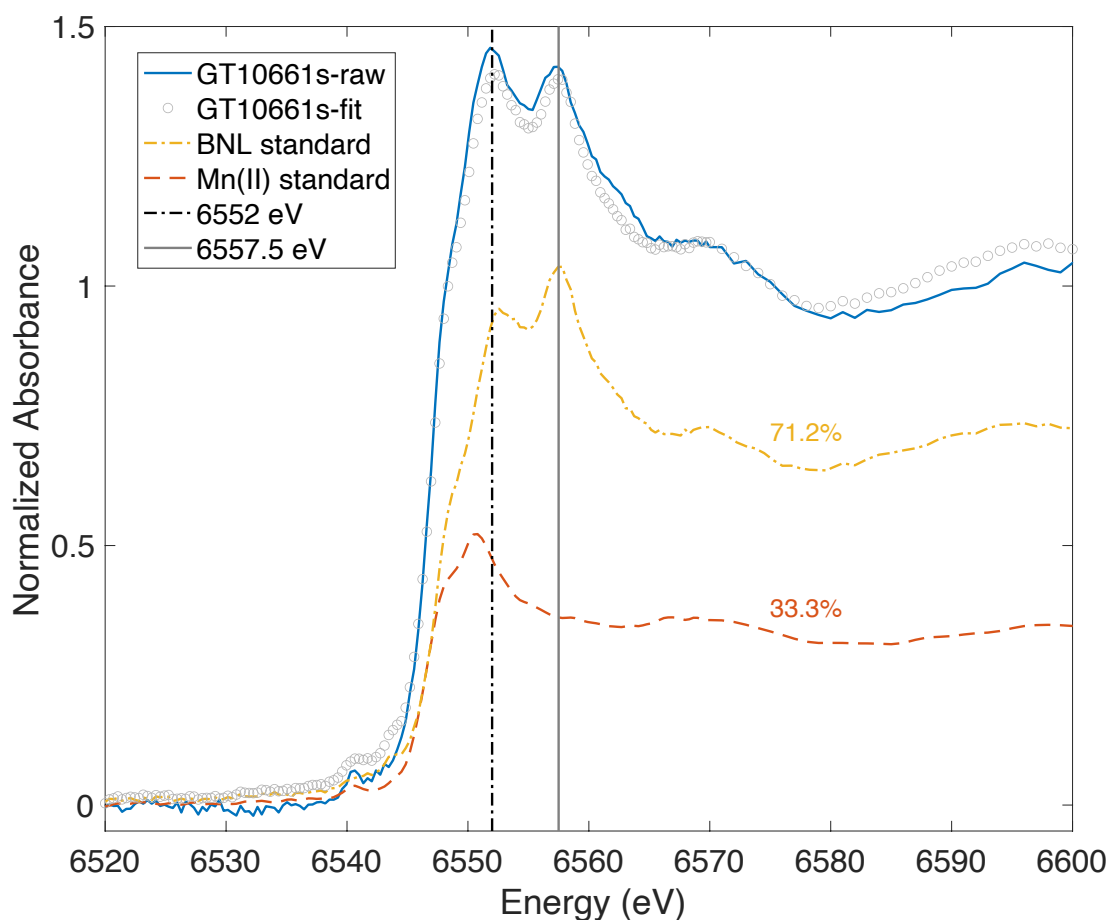
Figure S2. Linear combination fit (LCF) for surface sample GT10661s at Station 6 with the benthic nepheloid layer (BNL) sample (GT12276s), Mn(II) (GT11010s), Mn(III) (feitknechtite), and Mn(IV) (δ-MnO$_2$) references in the LCF. The fraction of the BNL reference (assumed to be Mn silicates) in the fit is 71.20% (68.11% if normalized to 1), and Mn(II) (GT11010s) is 33.34% (31.89% if normalized to 1). The fractions of feitknechtite and δ-MnO$_2$ are negligible. The R factor is 0.0014. Vertical black dash-dot and grey solid lines at 6552 eV and 6557.5 eV, respectively, for reference.
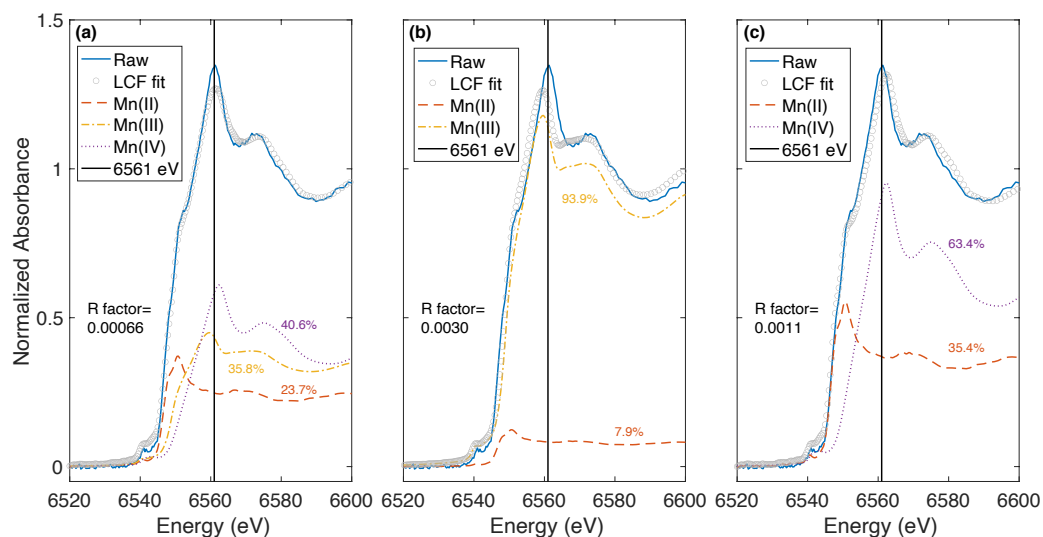
Figure S3. Linear combination fit for oxidized sample GT12240s at Station 60 with (a) Mn(II) (GT11010s), Mn(III) (feitknechtite), and Mn(IV) (δ-MnO$_2$) references, (b) GT11010s and feitknechtite only, and (c) GT11010s and δ-MnO$_2$ only in the fit. The fractions for different references (not normalized to 1) and R factor for the fit are displayed in each subplot. Better fits are characterized by smaller R factors. Vertical black solid lines at 6561 eV for reference.
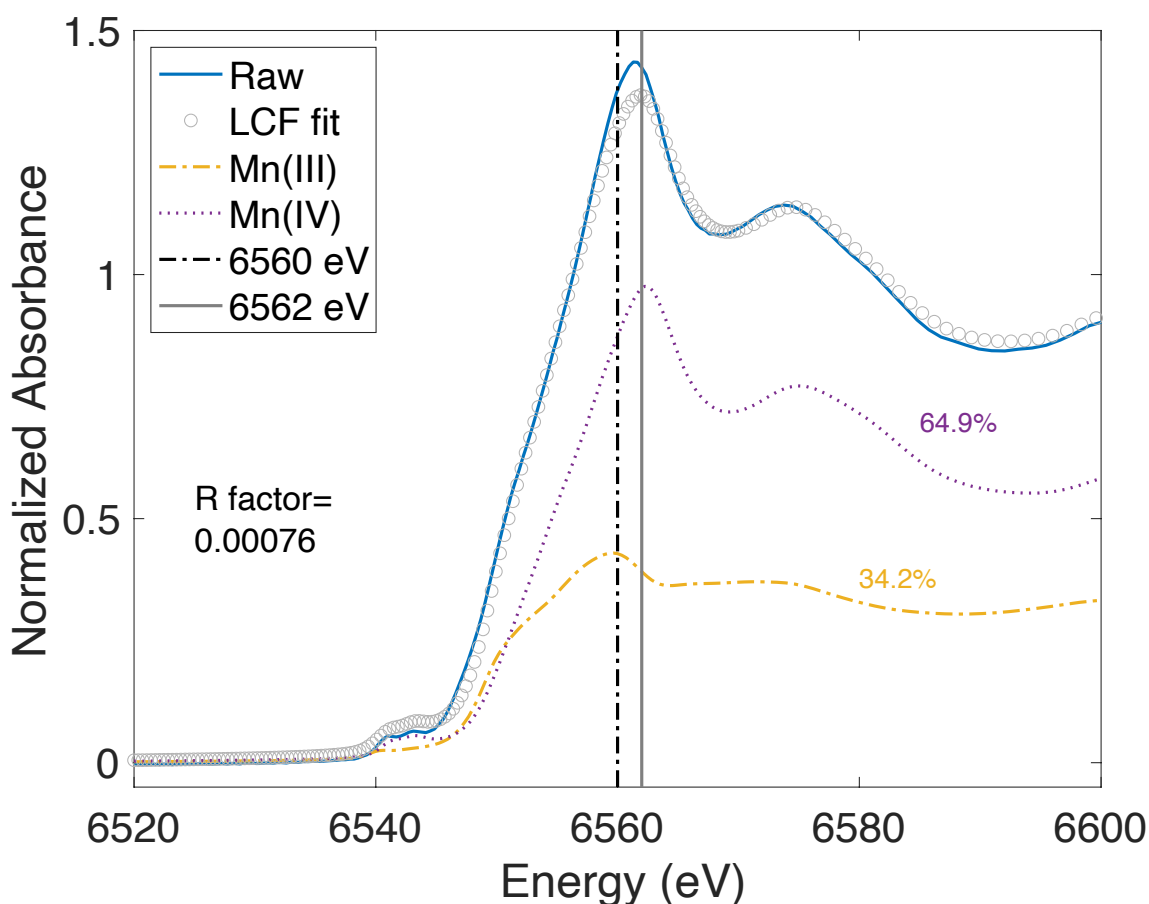
Figure S4. Linear combination fit for the most oxidized sample GT10800s in the halocline at Station 14 using Mn(III) (feitknechtite), and Mn(IV) (δ-MnO$_2$) as Mn references. The fit fractions for different references and R factor for the fit are displayed. Vertical black dash-dot and grey solid lines at 6560 eV and 6562 eV, respectively, for reference.
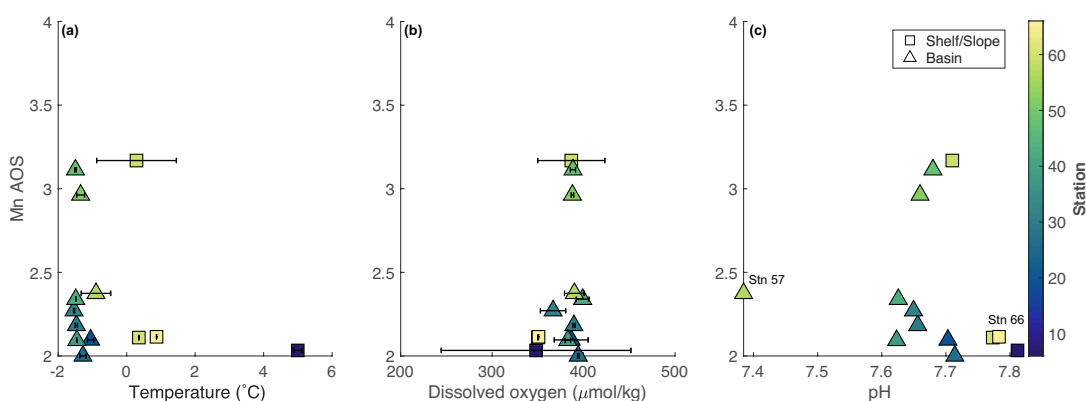

Figure S5. Scatter plots between Mn Average Oxidation State (AOS) from pumps and hydrographic parameters (a) Temperature (˚C); (b) dissolved oxygen (μmol/kg); (c) pH from the CTD rosette at pressure = 20 decibars. Mn AOS were determined on particles collected from pump

casts. Temperature and oxygen were collected from sensors mounted on the ODF CTD rosette and are plotted as the mean (marker) and standard deviation (error bars) of all CTD casts (N=1-7) from that station; pH was determined from discrete samples from one of the ODF CTD casts (Woosley et al., 2017) and linearly interpolated to 20 decibars. The multiple ODF CTD casts at each station generally spanned a similar range of light conditions as experienced by pump casts, so the mean and range should be a good indication of temperature and dissolved oxygen during particle sampling. Underway surface seawater measurements give additional evidence about the minor diel variation of temperature and dissolved oxygen in the Western Arctic Ocean, especially in the basin (data not shown). Measurements of pH were only made from one ODF CTD cast, but this was fortuitously frequently at similar light conditions as the pump cast, except for stations 57 and 66, when the pH data were from nighttime and the pump casts were during the day. The lowest pH observed at 20 decibars is from Station 57 (7.38), but it may not indicate strong remineralization in-situ at night, since the pH values measured at night in the surface of more productive slope Station 60 and shelf Station 66 are both higher than 7.65. Such low pH values can be reached within the strong benthic nepheloid layer (BNL) at shelf Station 61. Likely, the large pH difference between Station 57 and other basin station is due to lateral transport of a low pH water mass from the shelf BNL to Station 57.
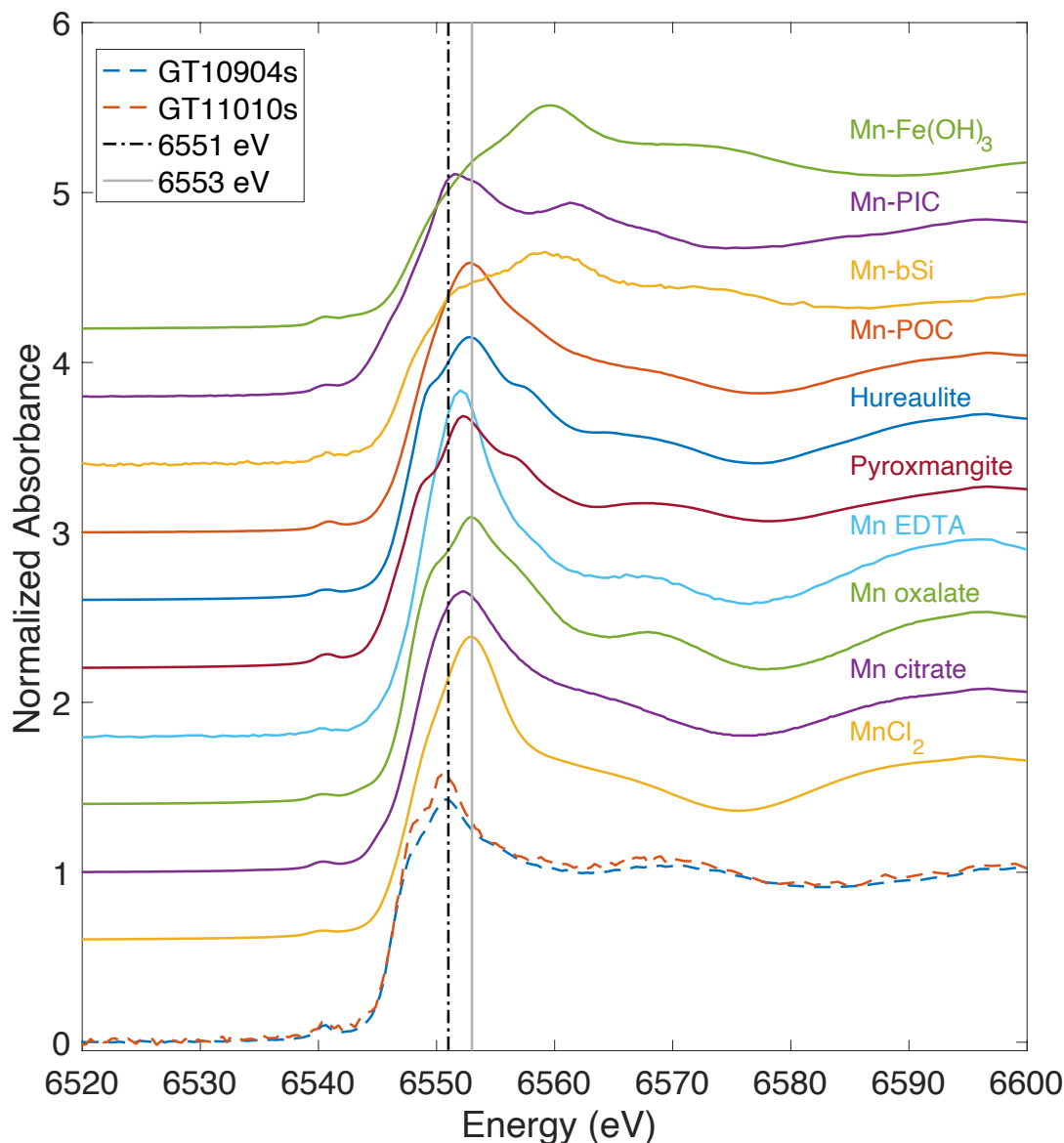
Figure S6. XANES spectra of the two most reduced surface samples, GT11010s at Station 26 and GT10904s at Station 19 (spectra with dashed lines) and six Mn(II) mineral references and four $MnCl_2$ adsorption standards (spectra with solid lines). Mn(II) references plotted include inorganic Mn ($MnCl_2$), organically bound Mn (Mn-citrate, -oxalate, and -EDTA), Mn silicates (Pyroxmangite), and Mn phosphates (Hureaulite). Mn-citrate and -oxalate spectra were obtained at the Australian Synchrotron (Blamey et al., 2018). We applied +1 eV energy shift observed in hausmannite ($Mn^{II}Mn^{III}_2O_4$) XANES spectrum to correct for the energy difference between SSRL and the Australian Synchrotron. Mn EDTA was measured at the Brazilian Synchrotron Light Laboratory (LNLS) (Machado et al., 2019). No obvious energy offset was observed between SSRL and LNLS based on Mn foil standards. Sorbed Mn standards we made and ran at Beamline 11-2 at SSRL include four major particle phases, particulate organic carbon (POC) from cultures of green algae,

clean diatom frustules, particulate inorganic carbon (PIC) from cleaned foraminifera shells, and synthesized 2-line ferrihydrite (Lee et al., 2021). Vertical black dash-dot and grey solid lines at 6551 eV and 6553 eV, respectively, for reference.
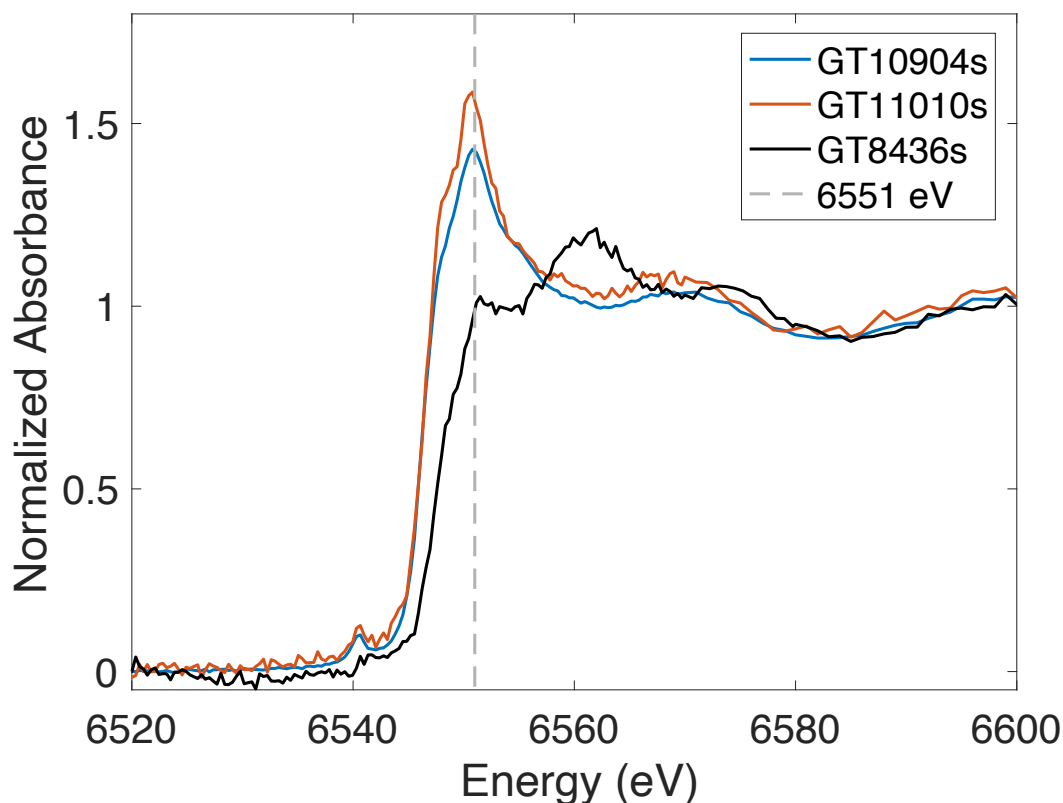

Figure S7. XANES spectra of the two most reduced surface samples, GT11010s at Station 26 and GT10904s at Station 19 in the GN01, and the unknown Mn mineral that contains pMn(II) in a neutrally buoyant hydrothermal plume from 15°S East Pacific Rise collected from the U.S. GEOTRACES GP16 cruise (Lee et al., 2021).

Table S1. Sampling locations, light conditions, and particulate Mn concentration and average oxidation state of particles collected by in-situ pumps in the surface of the Western Arctic Ocean (uploaded separately).

Name	White line position	Sources
GT11010s (the most reduced surface sample)	6551 eV	This study
Mn adsorption standard (particulate inorganic carbon)	6552 eV	Lee et al. (2021)
Pyroxmangite	6552 eV	Lee et al. (2021)
Mn(II) citrate_PK	6552 eV	Blamey et al. (2018)
Mn(II) EDTA_HC	6552 eV	Machado et al. (2019)
Mn adsorption standard (particulate organic carbon)	6553 eV	Lee et al. (2021)
Hureaulite	6553 eV	Lee et al. (2021)
MnCl$_2$_CH	6553 eV	Learman et al. (2011)
Mn(II) oxalate_PK	6553 eV	Blamey et al. (2018)
Mn(II)-Siderophores	6553 eV	Harrington et al. (2012)
Mn-SOD	6554 eV	Gunter et al. (2006)
Mn adsorption standard (biogenic silica)	6559 eV	Lee et al. (2021)
Mn adsorption standard (ferrihydrite)	6560 eV	Lee et al. (2021)

Table S2. Summary of white line positions for Mn superoxide dismutase (SOD), adsorbed, inorganic and organically bound Mn XANES reference spectra. No references were found with a white line as low as observed for GT11010s.

Reference name	Formula
Mn(II) oxide	$Mn^{II}O$
Mn(II) sulfide	$Mn^{II}S$
Hureaulite	$Mn^{II}_5(PO_3OH)_2(PO_4)_2 \cdot 4H_2O$
Pyroxmangite	$Mn^{II}SiO_3$
Chalcophanite_CH	$ZnMn^{IV}_3O_7 \cdot 3H_2O$
δ-MnO$_2$_CH	$δ$-$Mn^{IV}O_2$
Feitknechtite_CH	$Mn^{III}O(OH)$
GT11010s-Mn(II)	Unknown Mn(II) phases
Hausmannite_CH	$Mn^{II}Mn^{III}_2O_4$
Manganese chloride_CH	$Mn^{II}Cl_2$
Mn foil_CH	Mn^0
Mn citrate_PK	Mn(II)-citrate
Mn oxalate_PK	Mn(II)-oxalate
Mn EDTA_HC	Mn(II)-EDTA
DBK1 spessartine_22_24_fl_JJ	$Mn^{II}_3Al_2(SiO_4)_3$
Hotazel_Braunite_009_fl_JJ	$Mn^{II}Mn^{III}_6(SiO_4)O_8$
PiemontiteGRR_039_fl_JJ	$\{Ca_2\}\{Al_2Mn^{III}\}(Si_2O_7)(SiO_4)O(OH)$
PiemontitieGRR_2_040_fl_JJ	$\{Ca_2\}\{Al_2Mn^{III}\}(Si_2O_7)(SiO_4)O(OH)$

Table S3. Mn mineral references in the current library (N=18). See Text S1 for further details.

Table S4. Mn XANES spectra sample and reference spectra used in the calculation of Mn average oxidation state (uploaded separately).